batteries

MDPI

Article

State-of-Charge and State-of-Health Estimation in Li-Ion Batteries Using Cascade Electrochemical Model-Based Sliding-Mode Observers

Yong Feng [1], Chen Xue [1], Fengling Han [2,*], Zhenwei Cao [3] and Rebecca Jing Yang [4]

[1] School of Electrical Engineering and Automation, Harbin Institute of Technology, Harbin 150001, China; yfeng@hit.edu.cn (Y.F.); xuechen@stu.hit.edu.cn (C.X.)
[2] School of Computing Technologies, RMIT University, Melbourne, VIC 3000, Australia
[3] School of Science, Computing and Engineering Technologies, Swinburne University of Technology, Melbourne, VIC 3122, Australia; zcao@swin.edu.au
[4] School of Property Construction and Project Management, RMIT University, Melbourne, VIC 3000, Australia; rebecca.yang@rmit.edu.au
* Correspondence: fengling.han@rmit.edu.au; Tel.: +61-3-9925-3402

Abstract: This paper proposes a cascade approach based on a sliding mode observer (SMO) for estimating the state of charge (SoC) and state of health (SoH) of lithium-ion (Li-ion) batteries using a single particle model (SPM). After convergence, the observation error signal of the current node in the cascade observer is generated from the output injection signal of the previous node's observer. The current node's observer generates its output injection signal, leading to its convergence. This sequential process accurately determines the observed values of each node using only the battery's current and voltage. Subsequently, the SoC and SoH are estimated using observations of lithium-ion concentrations on the surface and inside the battery anode. The accuracy of this approach is validated using Dynamic Stress Test (DST) and Federal Urban Driving Scheme (FUDS) experimental data. A comparative analysis with conventional SMO and Extended Kalman Filter (EKF) algorithms demonstrates the approach's effectiveness and superior performance, confirming its practical applicability.

Keywords: Li-ion batteries; single-particle model (SPM); sliding-mode observers; state of charge; state of health

Citation: Feng, Y.; Xue, C.; Han, F.; Cao, Z.; Yang, R.J. State-of-Charge and State-of-Health Estimation in Li-Ion Batteries Using Cascade Electrochemical Model-Based Sliding-Mode Observers. *Batteries* **2024**, *10*, 290. https://doi.org/10.3390/batteries10080290

Academic Editors: Carlos Ziebert and Federico Baronti

Received: 4 July 2024
Revised: 25 July 2024
Accepted: 7 August 2024
Published: 15 August 2024

1. Introduction

Amid the global shift toward sustainable energy, electric vehicles (EVs) have risen as a viable solution to environmental concerns, the greenhouse effect, and the reliance on fossil fuels. Lithium-ion (Li-ion) batteries, known for their high energy density and longevity, have become central to the energy storage systems of EVs. This transition has positioned EV battery systems (EVBS) as a crucial area for Li-ion battery applications. Additionally, Li-ion batteries play a fundamental role in battery energy storage systems (BESS), which are essential for supporting renewable energy infrastructure.

Li-ion batteries are typically configured in series or parallel within EVBS and BESS to meet energy system requirements. Maintaining batteries within their operating range is a huge challenge and requires precise monitoring to prevent conditions such as overcharging or over-discharging. The key to accurate battery monitoring is to obtain the battery's state of charge (SoC) and state of health (SoH), which cannot be directly measured online and can only be estimated through voltage- and current-based algorithms.

Battery model-based methods are the most accurate and popular for estimating Li-ion batteries' State of Charge (SoC) and State of Health (SoH). Commonly used models include data-driven models (DDM) [1], equivalent circuit models (ECM) [2], and electrochemical models (EM) [3]. DDM, which relies on training data without mathematical models,

may compromise accuracy. EECM employs circuit elements to represent the battery's internal structure, offering a simplified and computationally efficient model, though it is less accurate than EM. EM provides detailed insights by examining the electrochemistry and lithium-ion movements within batteries, but its complexity can hinder practical applications [4]. The single particle model (SPM) and its extended version (ESPM) are prominent within EMs. ESPM offers detailed insights at the expense of increased complexity [5]. In contrast, SPM focuses on core battery dynamics, offering a balance of simplicity and computational efficiency, suitable for applications requiring quick calculations and straightforward implementations.

Traditionally, the Kalman filter (KF) and its nonlinear variant Extended KF (EKF) have been widely used in practice and have become the first choice for SoC and SoH estimation due to their simplicity, optimality, and robustness [4,6,7]. However, they also suffer from some drawbacks, such as sensitivity to initial conditions, reliance on Gaussian noise assumptions, and high computational intensity, which illustrates the need to develop new SoC and SoH estimation algorithms for Li-ion batteries.

The sliding mode observer (SMO) applies sliding mode control (SMC) technology to provide a viable alternative for SoC and SoH estimation. SMO is robust to parameter variations and external disturbances, ensures finite-time convergence, and exhibits adaptability and ease of implementation. Recent research has explored the application of SMOs in Li-ion battery SoC/SoH estimation. For example, in [8], the Luenberger observer is used with SMO to estimate the SoC of Li-ion batteries using reduced-order SPM. In [9], a nonlinear adaptive SMO is designed to estimate the SoC, electrode particle stress, and solid-phase diffusivity of Li-ion batteries against SPM and single-particle mechanical stress models. In [10], an interconnected SMO is proposed to simultaneously estimate the cathode's and anode's volume and surface concentrations. In [11], adaptive interconnect SMO to estimate the SoC accurate battery capacity. Despite the potential of SMO for Li-ion battery state estimation, existing SMO applications face several challenges, including:

1. Observation errors often converge to a bounded region rather than zero, thus requiring an increase in gain, which may cause estimation oscillations.
2. The uniform sign function in state variables limits the choice of observer parameters and creates homogeneity, which affects the observer's accuracy.
3. Current SMOs typically achieve asymptotic rather than finite-time convergence, but the error increases due to the higher order of EM and the recursive estimation form.

This paper proposes a cascade SMO method for SoC and SoH estimation. An SMO is first designed to observe the lithium-ion concentration on the battery anode surface. Then an integrated terminal SMO (ITSMO) is designed to observe the lithium-ion concentration inside the anode. Finally, these observed lithium-ion concentrations are used to estimate the SoC accurately. In addition, a low-pass filter is used to form a battery voltage-augmented system, and an SMO of the battery voltage is designed to achieve battery capacity and SoH estimation. Contributions of this paper include:

1. A novel cascade SMO estimation method tailored for Li-ion battery SPMs improves the accuracy of battery state estimation.
2. An augmented battery output voltage equation is constructed through a low-pass filter, laying a solid foundation for SoH estimation.
3. Fast and accurate SoC and SoH estimation is achieved utilizing finite-time anode lithium-ion concentration estimation.

The unique structure and characteristics of the cascade SMO help the estimation method proposed in this paper quickly and accurately estimate the SoC and SoH of lithium-ion batteries. This will allow Li-ion battery applications to operate more efficiently, extend service life, and improve safety standards, potentially revolutionizing battery management systems. The approach has particular implications for EV applications and renewable energy battery storage systems, marking a critical step in deploying and managing sustainable energy solutions.

The paper is structured as follows: Section 2 introduces the SPM model of Li-ion batteries considering capacity degradation and power fade. Section 3 details the design of an anode surface lithium-ion concentration observer and a cascade observer for remaining anode nodes. Section 4 introduces an SoH estimation algorithm combining filtered voltage and current. Section 5 validates the proposed method through experimental results. Finally, Section 6 concludes the paper.

Notation: Throughout, superscripts $^+$ and $^-$ denote parameters or states in the positive and negative electrodes, respectively, while $^\pm$ refers to either electrode.

2. Problem Formulation and Preliminaries

EMs are a fundamental tool for understanding the complex chemical and physical processes that occur during the operation of Li-ion batteries. Notable among these models are the pseudo-two-dimensional (P2D) model [12], the single-particle model (SPM) [13] and the extended SPM (ESPM) [14]. The P2D model is recognized for its complexity and detailed representation, making it ideal for in-depth battery research, but it demands substantial computational resources. The ESPM, on the other hand, balances modeling accuracy and computational efficiency, making it well-suited for advanced simulation tasks. In contrast, the SPM provides a simpler approximation of cell dynamics that requires minimal computational resources. Table 1 lists the comparative analysis of three EMs and the Equivalent Circuit Model (ECM). Since this paper focuses on observer design, the SPM is chosen as the preferred EM for Li-ion batteries. This choice is based on the simplicity and computational efficiency of SPMs, which are advantageous for observer design and offer more accuracy than ECMs.

Table 1. Comparison of Four Models.

Model	P2D	ESPM	SPM	ECM
Equations	PDEs	PDEs	ODEs	ODEs
Computational cost	High	Moderate	Low	Low
Implementation complexity	High	Moderate	Low	Low
Design complexity	High	Moderate	Low	Low
Insight into battery dynamics	Very high	High	Moderate	Low
Parameter identification ease	Low	Moderate	High	High
Accuracy	Very high	High	Moderate	Low
Suitability for observer design	Limited	Limited	Yes	Yes
Real-time applications	Limited	Moderate	High	High

The structure of the SPM is illustrated in Figure 1, where the positive and negative electrodes are represented as anode and cathode spherical particles, respectively. The lithium-ion concentration in the electrodes is denoted by $\boldsymbol{c}_s^\pm = [c_{s,1}^\pm, c_{s,2}^\pm, \ldots, c_{s,n}^\pm]$. Each term $c_{s,i}^\pm, i = 1, 2, \ldots, n$ specifies the lithium-ion concentration at a specific node. The lithium-ion concentration distribution on the anode and cathode spherical particles is divided into n nodes. The choice of n is critical; a higher n enhances model accuracy and increases computational load. Therefore, choosing n requires careful consideration to balance accuracy and computational feasibility for practical applications. The n-th order SPM of a Li-ion battery can be succinctly described by the state equation and output equation as follows [8]:

$$\begin{cases} \dfrac{dc_{s,n}^{-}}{dt} = \varphi\left(\dfrac{n-1}{n}c_{s,n-1}^{-} - \dfrac{n-1}{n}c_{s,n}^{-}\right) - b_n I \\ \dfrac{dc_{s,i}^{-}}{dt} = \varphi\left(\dfrac{i-1}{i}c_{s,i-1}^{-} - 2c_{s,i}^{-} + \dfrac{i+1}{i}c_{s,i+1}^{-}\right), \ i = n-1, \cdots, 2 \\ \dfrac{dc_{s,1}^{-}}{dt} = \varphi\left(-2c_{s,1}^{-} + 2c_{s,2}^{-}\right) + d \end{cases} \tag{1}$$

$$\begin{aligned} V_t = & \frac{R_g T}{\alpha^{+} F}\sinh^{-1}\left(\frac{-0.5I}{a_s^{+} A L^{+} i_0^{+}(c_{s,n}^{-})}\right) + U^{+}(c_{s,n}^{-}) \\ & - \frac{R_g T}{\alpha^{-} F}\sinh^{-1}\left(\frac{0.5I}{a_s^{-} A L^{-} i_0^{-}(c_{s,n}^{-})}\right) - U^{-}(c_{s,n}^{-}) - R_f I \end{aligned} \tag{2}$$

where $c_{s,0}^{-} = 0$, $b_n = (1+n)/n\Delta^{-} F a_s^{-} A L^{-}$, $\varphi = D_s^{-}/\Delta^{-2}$, $\Delta^{-} = R_s^{-}/n$, D_s^{-} is the diffusion coefficient of lithium-ions in the cathode, R_s^{-} is the radius of the cathode's spherical particle, I is the current, R_f is the internal resistance, and F is the Faraday constant. The specific interface surface area for the cathode is represented by a_s^{-}, while A indicates the current collection area. L^{-} is the domain thickness in the cathode. Lastly, d represents the unknown model uncertainty. Although its exact value is unidentified, it can be assumed to be bounded and Lipschitz continuous, i.e., $|d| \leq D$ and $|\dot{d}| \leq F_d$, where D and F_d are two known positive constants.

Let $\boldsymbol{c}_s^{-} = [c_{s,1}^{-}, \ldots, c_{s,n}^{-}]^T$. Rewriting (1) and (2), we have:

$$\dot{\boldsymbol{c}}_s^{-} = \boldsymbol{f}(\boldsymbol{c}_s^{-}) - [0, \ldots, 0, b_n]^T I + \boldsymbol{b}_d d \tag{3}$$

$$V_t = h(c_{s,n}^{-}, I) - R_f I \tag{4}$$

where $\boldsymbol{b}_d = [b_{d1}, \cdots, b_{dn}]^T = [1, 0, \cdots, 0]^T$. Two functions $\boldsymbol{f}(\boldsymbol{c}_s^{-})$ and $h(c_{s,n}^{-}, I)$ relate to the terms in (1) and (2).

This paper aims to refine SoC and SoH estimation algorithms in NMC Li-ion batteries using the SPM and cascade SMOs, addressing existing gaps in battery state estimation methodologies.

We introduce preliminary findings that pave the way for the primary results in the paper.

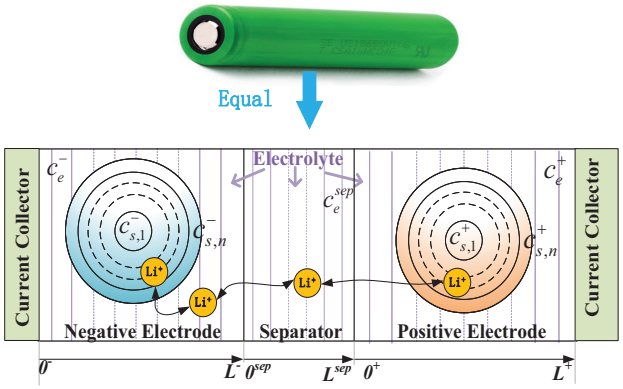

Figure 1. Modelling of a Li-ion battery.

Lemma 1. *A monotonic relationship [8] exists between the battery's output voltage and the anode's surface lithium-ion concentration for any given current I as expressed in:*

$$\operatorname{sgn}\left(h(c_{s,n}^{-(1)}, I) - h(c_{s,n}^{-(2)}, I)\right) = \operatorname{sgn}(c_{s,n}^{-(1)} - c_{s,n}^{-(2)}) \tag{5}$$

where $c_{s,n}^{-(1)}$ *and* $c_{s,n}^{-(2)}$ *denote two different values of the lithium-ion concentration on the surface of the anode.*

Lemma 2 ([15]). *Consider an nth-order system* $\dot{\boldsymbol{x}} = \boldsymbol{f}(\boldsymbol{x})$*, where* $\boldsymbol{f}(0) = 0$ *and* $\boldsymbol{x} \in R^n$*. If there exists a continuous positive definite function* $V(\boldsymbol{x}) > 0$*, and an open neighborhood of the origin* $\boldsymbol{x} = 0$ *such that* $\dot{V}(\boldsymbol{x}) \leq -\gamma V^{\lambda}(\boldsymbol{x})$*, where* $\gamma > 0$ *and* $\lambda \in (0, 1)$*, then the system can converge to its equilibrium within a finite time* t_r *given by:*

$$t_r \leq \frac{1}{\gamma(1-\lambda)} V^{1-\lambda}(\boldsymbol{x}(\lambda)) \tag{6}$$

3. Cascade Observer for SoC/SoH Estimation

The framework on SoC/SoH estimation algorithms begins by constructing an observer to estimate the lithium-ion concentration at the anode's n-th node, specifically on the anode's surface, denoted as $c_{s,n}^{-}$. The resulting estimate, $\hat{c}_{s,n}^{-}$, becomes an auxiliary input for an $(n-1)$-order cascade observer focused on the internal lithium-ion concentration of the anode. Moreover, this estimate also assists as an auxiliary input for the SoC and SoH estimators.

The $(n-1)$-order cascade lithium-ion concentration observer consists of $(n-1)$ node observers. Specifically, the i-th node observer acquires its observation error estimate from the $(i+1)$-th node observer and employs this information to minimize its observation error to zero, with i ranging from $(n-1)$ down to 1. Once all nodes within this $(n-1)$-order cascade lithium-ion concentration observer reach a zero observation error, the concentration states of the $(n-1)$ cathode nodes are determined, represented as $\hat{c}_{s,1}^{-}, \ldots, \hat{c}_{s,n-1}^{-}$.

Following this, the SoC estimator leverages the lithium-ion concentration estimates of the n nodes, $\hat{c}_{s,1}^{-}, \ldots, \hat{c}_{s,n}^{-}$, to compute the SoC estimate as per (17). Concurrently, the adaptive SoH estimator incorporates a low-pass filter to form an augmented system, as depicted in (21). This system characterizes the dynamic process of V_t and aids in the SoH estimation over slower time scales compared to designated aging parameters, exemplified in (22).

3.1. Anode Surface Lithium-Ion Concentration Observer

This study aims to estimate the lithium-ion concentration on the surface of the anode, specifically at its n-th node, denoted as $c_{s,n}^{-}$ in (1). We introduce an SMO structured as follows:

$$\begin{cases} \dot{\hat{c}}_{s,n}^{-} = -\varphi\left(1 - n^{-1}\right)\left(\hat{c}_{s,n}^{-} - \hat{c}_{s,n-1}^{-}\right) - b_n I + v_n \\ \hat{V}_t = h(\hat{c}_{s,n}^{-}, I) - R_f I \end{cases} \tag{7}$$

where $\hat{c}_{s,n}^{-}$ and $\hat{c}_{s,n-1}^{-}$ represent the estimates of $c_{s,n}^{-}$ and $c_{s,n-1}^{-}$, respectively. Additionally, v_n signifies the output injection affiliated with the anode surface concentration observer.

Considering the estimation errors for

$$\dot{e}_{s,n} = -\varphi\left(1 - n^{-1}\right)(e_{s,n} - e_{s,n-1}) - v_n \tag{8}$$

Theorem 1. *For the anode surface lithium-ion*

$$v_n = \left(\varphi(1 + c_{s,max}^{-})(1 - n^{-1}) + \eta_s\right) \operatorname{sgn}(e_V) \tag{9}$$

where $e_V = V_t - \hat{V}_t$ *is the voltage estimation error, and* $\eta_s > 0$ *is set as a design parameter. Should* e_V *reach zero within a finite duration, the estimation error for the subsequent observer* $\hat{e}_{s,n-1}$ *can be deduced using a low-pass filter as:*

$$T_s \dot{\hat{e}}_{s,n-1} + \hat{e}_{s,n-1} = \varphi^{-1} n (n-1)^{-1} v_n \tag{10}$$

with $T_s > 0$ being another design parameter.

Proof. Consider the candidate Lyapunov function $V_s = 0.5e_{s,n}^2$. Differentiating it with time t and using Lemma 1, we obtain:

$$\begin{aligned}\dot{V}_s &= e_{s,n}\dot{e}_{s,n}\\ &= -\varphi\left(1-n^{-1}\right)e_{s,n} + \varphi\left(1-n^{-1}\right)e_{s,n-1}e_{s,n} - e_{s,n}v_n\\ &= -\varphi\left(1-n^{-1}\right)e_{s,n} + \varphi\left(1-n^{-1}\right)e_{s,n-1}e_{s,n} - e_{s,n}\left(\varphi(1+c_{s,max}^{-})\left(1-n^{-1}\right)+\eta_s\right)\mathrm{sgn}e_V\end{aligned}$$

It can be obtained from (5) and (7) as follows:

$$\mathrm{sgn}e_V = \mathrm{sgn}(h(c_{s,n}^{-}, I) - h(\hat{c}_{s,n}^{-}, I)) = \mathrm{sgn}(e_{s,n})$$

hence,

$$\dot{V}_s \le \varphi\left(1-n^{-1}\right)|e_{s,n}| + \varphi\left(1-n^{-1}\right)|e_{s,n-1}e_{s,n}| - \left(\varphi(1+c_{s,max}^{-})\left(1-n^{-1}\right)+\eta_s\right)|e_{s,n}|$$

Note that $c_{s,n-1}^{-}$ is defined over the range: $c_{s,n-1}^{-} = \left\{c \in R | 0 \le c \le c_{s,max}^{-}\right\}$. This implies that $|e_{s,n-1}| \le c_{s,max}^{-}$. From this, the relationship follows:

$$\dot{V}_s \le -\left(\varphi(1+c_{s,max}^{-})\left(1-n^{-1}\right)+\eta_s\right)|e_{s,n}| + \varphi(1+c_{s,max}^{-})\left(1-n^{-1}\right)|e_{s,n}| \le -\eta_s|e_{s,n}|$$

Then, $\dot{V}_s \le -\eta_s\sqrt{2}V_s^{1/2}$.

Leveraging Lemma 2, it can be deduced that the error dynamics (8) converges to $e_{s,n} = 0$ within a finite time, $t_s \le \sqrt{2}\eta_s^{-1}|e_{s,n}(0)|$. Afterward, $e_{s,n}$ remains at zero. Thus, for $t \ge t_s$, we derive from (8):

$$\varphi\left(1-n^{-1}\right)e_{s,n-1} = v_n$$

which simplifies to:

$$e_{s,n-1} = \varphi^{-1}n(n-1)^{-1}v_n$$

Given that the bandwidth of v_n significantly surpasses that of $c_{s,n}^{-}$, we can employ a low-pass filter to determine an estimate of $c_{s,n}^{-}$ in (10). The proof is thus completed. □

3.2. Lithium-Ion Concentration Estimation within the Anode

In the previous section, we focused on the design of the n-th node observer. Once the estimation error of this observer converges to zero within a finite time, the estimation error of the $(n-1)$-th node observer $\hat{e}_{s,n-1}$ will appear. It is driven by the output injection signal of the n-th node observer and can be obtained through a low-pass filter according to (10).

After determining the estimate $\hat{e}_{s,n-1}$, we can further design the observer for the $(n-1)$-th node. Its output injection function v_{n-1} is designed using $\hat{e}_{s,n-1}$, aiming to drive the error of the $(n-1)$-th node observer to zero. Once this is achieved, the estimated error $\hat{e}_{s,n-2}$ for the $(n-2)$-th node observer can be obtained. Then, use this estimation error to design the output injection function v_{n-2} of the $(n-2)$-th node observer. This process continues until the first node observer. This cascading approach can systematically design all n node observers. Their entire design process can be succinctly summarized by a recursive equation as follows:

$$\frac{d\hat{c}_{s,i}^{-}}{dt} = \varphi\left(\frac{i-1}{i}\hat{c}_{s,i-1}^{-} - 2\hat{c}_{s,i}^{-} + \frac{i+1}{i}\hat{c}_{s,i+1}^{-}\right) + v_i\ ,\ \ i = n-1, \cdots, 1 \tag{11}$$

where $v_i, i = 1, \cdots, n-1$ denote the output injection signals.

Given the definition of estimation errors for the lithium-ion concentration inside the anode as $e_{s,i} = c_{s,i}^{-} - \hat{c}_{s,i}^{-}, i = 1, \cdots, n-1$, considering (1) and (11) yields:

$$\frac{de_{s,i}}{dt} = \varphi\left(\frac{i-1}{i}e_{s,i-1} - 2e_{s,i} + \frac{i+1}{i}e_{s,i+1}\right) + b_{di}d - v_i \ , \ \ i = n-1, \cdots, 1 \tag{12}$$

The error dynamics expressed above correspond to $n-1$ sliding-mode manifolds, defined as:

$$s_i = \dot{e}_{s,i} + \beta_i e_{s,i}^{\alpha_i} \ , \ \ i = n-1, \cdots, 1 \tag{13}$$

where $0 < \alpha_i < 1$ and $\beta_i > 0$ for $i = 1, \cdots, n-1$ provide the characteristics of the desired sliding motion dynamics.

Considering that the change in lithium-ion concentration within the anode electrode is gradual, it can be concluded that the relevant derivative is bounded. Since the output injections of cascade SMOs are designed to be continuous, the following assumptions can be made:

$$|\dot{e}_{s,i}| = \left|\dot{c}_{s,i}^{-} - \dot{\hat{c}}_{s,i}^{-}\right| \leq F_i \ , \ \ i = n-1, \cdots, 1 \tag{14}$$

where $F_i, i = 1, \cdots, n-1$ are predefined positive constants.

Theorem 2. *For the cascade observer defined by (7) and (11), the sliding surface of each i-th node is specified by (13). The i-th output injection signal is then given as:*

$$v_i = -2\varphi\hat{e}_{s,i} + \beta_i\hat{e}_{s,i}^{\alpha_i} + \int_0^t \left(\varphi F_i\frac{i-1}{i} + b_{di}F_d + \eta_i\right)\mathrm{sgn}s_i dt \ , \ \ i = n-1, \cdots, 1 \tag{15}$$

where $\eta_i > 0$, $\hat{e}_{s,n-1}$ and F_i are determined by (10) and (14), respectively. When the observer reaches the i-th sliding surface in finite time, the $(i-1)$-th observation error can be given by

$$\hat{e}_{s,i-1} = \int_0^t \left(F_i + \eta_i\varphi^{-1}\frac{i}{i-1}\right)\mathrm{sgn}s_i dt \ , \ \ i = n-1, \cdots, 2 \tag{16}$$

Once the observer synchronizes with all sliding surfaces, the errors will tend towards zero in finite time.

Proof. Substituting the error dynamics (12) into (13) gives

$$s_i = \varphi\left(\frac{i-1}{i}e_{s,i-1} - 2e_{s,i} + \frac{i+1}{i}e_{s,i+1}\right) + b_{di}d - v_i + \beta_i e_{s,i}^{\alpha_i}$$

Once the error dynamics of the $(i+1)$-th anode lithium-ion concentration cascade observer stabilize to zero, $e_{s,i+1}$ also converges to zero. Thus, this is expressed as $e_{s,i+1} = 0$. Given this condition, the above expression can be updated to:

$$s_i = \varphi\left(\frac{i-1}{i}e_{s,i-1} - 2e_{s,i}\right) + b_{di}d - v_i + \beta_i e_{s,i}^{\alpha_i}$$

Further, substituting (15) into the above formula yields

$$s_i = \varphi\frac{i-1}{i}e_{s,i-1} + b_{di}d - \int_0^t \left(\varphi F_i\frac{i-1}{i} + b_{di}F_d + \eta_i\right)\mathrm{sgn}s_i dt$$

Considering a candidate Lyapunov function $V_i = 0.5s_i^2$ and using assumption (8), it follows that

$$\begin{aligned}\dot{V}_i &= \left(\varphi\frac{i-1}{i}\dot{e}_{s,i-1}+b_{di}\dot{d}-\left(\varphi F_i\frac{i-1}{i}+b_{di}F_d+\eta_i\right)\mathrm{sgn}s_i\right)s_i\\ &\leq \varphi\frac{i-1}{i}|\dot{e}_{s,i-1}||s_i|-\left(\varphi F_i\frac{i-1}{i}+\eta_i\right)|s_i|\\ &\leq \varphi\frac{i-1}{i}F_i|s_i|-\left(\varphi F_i\frac{i-1}{i}+\eta_i\right)|s_i| \leq \eta_i|s_i|\end{aligned}$$

which implies that $\dot{V}_i \leq -\eta_i\sqrt{2}V_i^{1/2}$.

From Lemma 2, it can be concluded that the error dynamics of the i-th cascade observer can achieve $s_i = 0$ within a finite time denoted by t_i, specifically, $t_i \leq \sqrt{2}\eta_i^{-1}|s_i(0)|$, and subsequently maintain this state.

Consequently, for $s_i = 0, \forall t \geq t_i$, where $i = n-1, \cdots, 2$, we can further derive:

$$\varphi\frac{i-1}{i}e_{s,i-1}-\int_0^t\left(\varphi F_i\frac{i-1}{i}+\eta_i\right)\mathrm{sgn}s_i dt = 0$$

This directly corresponds to (16), thus finalizing the proof. □

3.3. SoC Estimation via Anode Lithium-Ion Concentration

The SoC provides a metric to determine the amount of charge present in a Li-ion battery compared to its maximum charge capacity. It is quantified as a percentage, varying between 0% (wholly discharged) and 100% (fully charged). Notably, the SoC of a Li-ion battery can be articulated in terms of the anode lithium-ion concentration, as depicted by (1) and (2). Specifically, the SoC can be defined as:

$$\mathrm{SoC} = \frac{\frac{3\Delta^{-2}}{R_s^{-3}c_{smax}^-}\sum_{i=1}^{n} i^2 c_{s,i}^- - \theta_{\min}^-}{\theta_{\max}^- - \theta_{\min}^-} \tag{17}$$

where R_s^- represents the radius of the anode spherical particle, as illustrated in Figure 1, and $\Delta^- = R_s^-/n$. z $\theta_{\max}^-$ and $\theta_{\min}^-$ denote the upper and lower stoichiometric points of the electrode lithium-ion concentration of the battery [7,9].

To accurately estimate the SoC of the Li-ion battery, one can first estimate the lithium-ion concentration on the surface and inside the anode using proposed cascade observers. Subsequently, the estimated values of lithium-ion concentration are used to determine the precise SoC of the Li-ion battery through (17).

4. Estimating SoH Using an Adaptive Mechanism

In addition to SoC, SoH is a crucial parameter for monitoring and managing Li-ion batteries. SoH ranges from 100% to 0% and indicates how much the power and energy capabilities of the battery have degraded since manufacturing.

Using the SPM of a battery, as detailed in (1) and (2), the SoH of the battery can be estimated. SoH is typically expressed as the capacity loss over the battery's lifetime, as follows:

$$\mathrm{SoH} = \frac{C_n}{C_{nominal}} \tag{18}$$

where $C_{nominal}$ represents the manufacturer-provided nominal capacity, and C_n denotes the current capacity as the battery ages. For precise SoH estimation, it is crucial to consider the time variance in R_f and C_n as outlined in (2). Specifically, the internal resistance of the battery R_f is defined as a function of C_n [16]:

$$R_f = R_f(C_n) = R_0 + R_{SEI}(C_n) + R_e(C_n) \tag{19}$$

where

$$R_{SEI}(C_n) = -\frac{R_s^- M_{SEI}(C_n - C_{nominal})}{6a_s^- A(L^-)^2 \kappa_{SEI} F \rho_{SEI} \varepsilon_s^-}$$

$$R_e(C_n) = -R_{e0} + \frac{L^+}{2A\kappa_{e^+}^{eff}} + \frac{L^{sep}}{A\kappa_{e^{sep}}^{eff}} + \frac{L^-}{2A\left(1 - \varepsilon_s^- - \frac{3\varepsilon_s^-}{R_s^-} + \frac{\varepsilon_s^- M_{SEI}(C_n - C_{nominal})}{6F\rho_{SEI}\varepsilon_s^- L^-} - \frac{\varepsilon_s^- L_{SEI0}}{R_s^-} - \varepsilon_f^-\right)^{1.5}}$$

From (19), we deduce that the terminal voltage of the battery V_t in (4) can be redefined as $V_t = h(c_{s,n}^-, I) - R_f(C_n)I$. To optimize SoH estimation, we incorporate augmented output dynamics into V_t:

$$T_t \dot{y} + y = V_t = h(c_{s,n}^-, I) - R_f(C_n)I \tag{20}$$

where y denotes the output from a low-pass filter, and T_t is a design parameter. It can be obtained from (20) that:

$$\dot{y} = -T_t^{-1} y + T_t^{-1} h(c_{s,n}^-, I) - T_t^{-1} R_f(C_n) I \tag{21}$$

An observer tailored for (21) is structured as:

$$\dot{\hat{y}} = -T_t^{-1} \hat{y} + T_t^{-1} h(c_{s,n}^-, I) - T_t^{-1} \hat{R}_f I + v_t \tag{22}$$

where $\hat{R}_f = R_f(\hat{C}_n)$, $\hat{C}_n$ is the estimate of C_n, and v_t refers to the output injection.

Defining the output estimation error as $e_y = y - \hat{y}$, it can be obtained from (21) and (22) as follows:

$$\dot{e}_y = -T_t^{-1} e_y - T_t^{-1}\left(R_f - \hat{R}_f\right) I - v_t \tag{23}$$

For the estimation error dynamics expressed by (23), the goal is to design the output injection v_t in (22) to be able to produce an ideal sliding motion on the sliding surface, expressed as

$$s_y = \dot{e}_y + \beta_y {e_y}^{\alpha_y} \tag{24}$$

where the parameters α_y and β_y are adjustable based on required performance.

Theorem 3. *The sliding surface defined in (24) combined with the following output injection guarantees the finite-time convergence of the error dynamics represented by (23):*

$$v_t = v_{t1} + v_{t2} \tag{25}$$

$$v_{t1} = -c e_y + \beta_y {e_y}^{\alpha_y} \tag{26}$$

$$v_{t2} = \int_0^t k_t \mathrm{sgn}(s_y) dt \tag{27}$$

where $k_t = T_t^{-1} R_d |I| + T_t^{-1} R_m |\dot{I}| + \eta_t$. *Once* $s_y = 0$ *is established, the power fade resistance can be deduced by*

$$\hat{R}_f = -\int_0^t k_{Rf} \mathrm{sgn}\left(I^{-1} \int_0^t k_t \mathrm{sgn}(s_y) d\tau\right) dt \tag{28}$$

Proof. Incorporating the output estimation error dynamics (23) into the sliding manifold (24), we get:

$$s_y = -T_t^{-1} e_y - T_t^{-1}\left(R_f - \hat{R}_f\right) I - v_t + \beta_y {e_y}^{\alpha_y}$$

Substituting the output injection signals of the observer (25) and (26) into the equation above gives

$$s_y = -T_t^{-1}\left(R_f - \hat{R}_f\right)I - v_{t2} \tag{29}$$

Differentiating s_y with time t, it can be obtained from (29) as follows:

$$\dot{s}_y = -T_t^{-1}\left(\dot{R}_f - \dot{\hat{R}}_f\right)I - T_t^{-1}\left(R_f - \hat{R}_f\right)\dot{I} - \dot{v}_{t2}$$

Choosing a Lyapunov function as $V_t = 0.5s_y^2$, and keeping in mind that $\dot{R}_f = 0$, it leads to:

$$\dot{V}_t = T_t^{-1}\dot{\hat{R}}_f I s_y - T_t^{-1}\left(R_f - \hat{R}_f\right)\dot{I}s_y - \dot{v}_{t2}s_y$$

Including (27) into the above equation gives:

$$\dot{V}_t = T_t^{-1}\dot{\hat{R}}_f I s_y - T_t^{-1}\left(R_f - \hat{R}_f\right)\dot{I}s_y - s_y k_t \mathrm{sgn}s_y$$

$$\leq T_t^{-1}\dot{\hat{R}}_f|I||s_y| + T_t^{-1}\left(R_f - \hat{R}_f\right)|\dot{I}||s_y| - k_t|s_y|$$

Reflecting upon the definition of k_t via (27), it can be obtained from the above expression:

$$\dot{V}_t = s_y\dot{s}_y \leq -\eta_t|s_y|$$

This validates that the system (23) can achieve $s_y = 0$ from any initial $s_y(0) \neq 0$ in a bounded time frame. When $s_y = 0$, as per (29), we ascertain:

$$R_f - \hat{R}_f = -T_t I^{-1} v_{t2} = -T_t I^{-1}\int_0^t k_t \mathrm{sgn}(s_y)dt$$

Thus, we get:

$$\mathrm{sgn}\left(R_f - \hat{R}_f\right) = -\mathrm{sgn}\left(I^{-1}\int_0^t k_t \mathrm{sgn}(s_y)dt\right) \tag{30}$$

By considering a Lyapunov function $V_R = 0.5(R_f - \hat{R}_f)^2$ and recognizing that $\dot{R}_f = 0$, a direct proof yields:

$$\dot{V}_R = \left(R_f - \hat{R}_f\right)\left(\dot{R}_f - \dot{\hat{R}}_f\right) = -\left(R_f - \hat{R}_f\right)\dot{\hat{R}}_f$$

By incorporating the derivative of (28) into the previous equation, we deduce:

$$\dot{V}_R = k_{Rf}\left(R_f - \hat{R}_f\right)\mathrm{sgn}\left(I^{-1}\int_0^t k_t \mathrm{sgn}(s_y)d\tau\right)$$

Acknowledging (30), the following can be derived:

$$\dot{V}_R = -k_{Rf}\left(R_f - \hat{R}_f\right)\mathrm{sgn}\left(R_f - \hat{R}_f\right) = -\sqrt{2}k_{Rf}V_R^{1/2}$$

This means that when the error dynamics (23) stays on the sliding surface $s_y = 0$, the estimate $\hat{R}_f$ can converge to the unknown R_f within a finite time, validating (28). This completes the proof. □

Remark 1. *Once s_y and $\hat{R}_f - R_f$ converge to zero in finite time, the value of $\hat{R}_f$ can be determined in the estimator given by (28). Given that it is expressed as a function of C_n in (19), then the estimate of C_n can be determined from the estimate of the power fade resistance, that is:*

$$\hat{C}_n = R_f^{-1}(\hat{R}_f) \tag{31}$$

From (30) and (31), the SoH of a Li-ion battery can be determined using: SoH $= \hat{C}_n / C_{nominal}$.

5. Experimental Verification

The method proposed in this paper is validated using experimental data from the NMC18650 Li-ion battery. The characteristics of this type of battery are LiNiMnCo positive electrode, graphite negative electrode, nominal capacity 2000 mAh, nominal voltage 3.6 V, and the upper and lower cut-off voltages are 4.2 V and 2.5 V respectively. The battery experimental system is shown in Figure 2. Battery experimental data comes from the Arbin BT2000 battery testing system used for dynamic stress testing (DST) or the Federal Urban Driving Scheme (FUDS) [17]. Charging and discharging of the battery are performed in a Yamato DVS402 environmental chamber to ensure a constant ambient temperature of 25°. Before starting the experiment, the battery was fully charged to the cut-off voltage 4.2 V using constant current and voltage. It was then continuously discharged at a rate of C/20 until it reached 80% capacity. This state serves as the starting point for all subsequent battery experimental data.

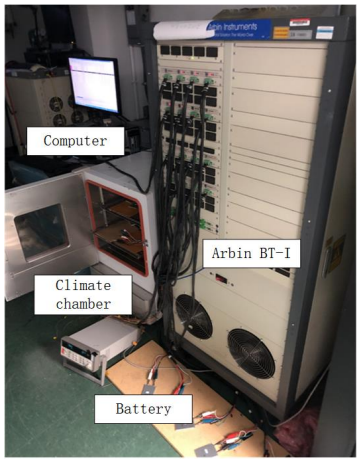

Figure 2. The battery experimental system.

The SPM of Li-ion batteries is defined by (1) and (2). In this paper, we choose the order of the model to be $n = 4$. The higher the order of SPM, the higher the accuracy of the model. However, modeling more parameters results in a higher order for the designed observer, making implementation more challenging. Given that the order of the ECM is 3rd order, it is appropriate to choose the order of SPM as 4. This choice demonstrates that the model accuracy of SPM is higher than that of the ECM, while also reducing the complexity of SPM, thereby easing the observer design. It should also be noted that the order of SPM can be appropriately increased as needed. The model parameters were determined using a genetic algorithm (GA) and experimental data on Li-ion batteries in DST. The final parameters of the battery SPM can be found in Table 2. For comparison, we also utilized an ECM of the battery built using the same experimental data as in SPM modeling. This ECM comes from our previous publication in [15]. The battery current experimental data is added to the inputs of both the ECM and SPM simultaneously. Then, the terminal voltage output of the battery is calculated based on these two models. The simulation results are shown in Figure 3. Comparing the terminal voltage output of the two models with the actual battery terminal voltage, it can be seen that SPM exhibits better accuracy than ECM. A key reason for this difference is that SPM is a fourth-order model, while ECM is a third-order model. It is worth noting that the order of SPM can be further improved, which means that its accuracy has the potential to be further improved. However, although SPM is superior to ECM in terms of accuracy, increasing the order of SPM will increase its computational complexity proportionally. Therefore, choosing the order of SPM requires a balance between model accuracy and computational complexity.

Table 2. SPM Model Parameters and States.

Parameter	Description	Value
A	current collector area [m^2]	0.1
$a_s^{\pm}$	specific interfacial surface area [m^2/m^3]	$2.100 \times 10^5/2.100 \times 10^5$
$c_{s,max}^{\pm}$	maximum electrode concentration [mol/m^3]	51,830/31,080
D_s^-	diffusion coefficient in electrode [m^2/s]	6.25×10^{-14}
F	Faraday's constant [C/mol]	96,485.4
$k_{i0}^{\pm}$	kinetics reaction rate constant [$Am^{2.5}mol^{-1.5}$]	$3 \times 10^{-7}/1 \times 10^{-7}$
$L^{+/sep/-}$	domain thickness [m]	$5 \times 10^{-5}/2 \times 10^{-5}/8 \times 10^{-5}$
R_g	universal gas constant [$Jmol^{-1}K^{-1}$]	8.314472
$R_s^{\pm}$	radius of active electrode particle [m]	$10^{-5}/10^{-5}$
T	temperature [K]	298.15
t_c^0	electrolyte transference number	0.4
$\alpha^{\pm}$	anodic, cathodic charge transfer coefficient	$1.8 \times 10^4/1.5 \times 10^4$
$\varepsilon_s^{\pm}$	active material volume fraction of electrode	0.6/0.5
$n_{s,Li}$	total moles of lithium in electrode [mol]	0.1679
$\theta_{max}^-, \theta_{min}^-$	stoichiometric points of electrode concentration	0.9/0.1
$U^{\pm}$	open circuit potential of electrode [V]	[14]
	Capacity and Resistance Fade parameters	
Parameter	Description	Value
$\varepsilon_f^{\pm}$	active volume fraction of filler/binder.	0.1/0.2
$\kappa_{e^{+/sep/-}}^{eff}$	effective electrolyte conductivity [S/m].	0.000324/0.002/0.000336
L_{SEI0}	initial SEI layer thickness [m]	5×10^{-9}
R_0	initial lumped resistance [Ω]	0.001
$C_{nominal}$	nominal capacity of the battery [Ah]	2
M_{SEI}	SEI layer molar mass [kg/mol]	78.89 [18]
ρ_{SEI}	SEI layer density [g/mol^3]	1690 [16]
κ_{SEI}	SEI ionic conductivity [S/m]	17.5×10^{-5} [16]

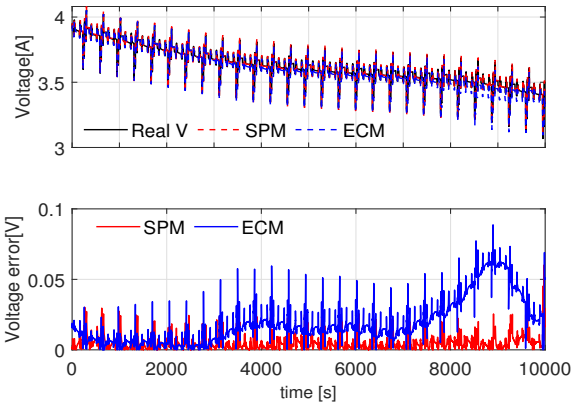

Figure 3. Test of SPM and ECM models.

The next step is to design a Li-ion battery SoC estimation algorithm. First, Theorem 1 is applied to design an SMO to estimate the lithium-ion concentration on the battery anode surface. Then, Theorem 2 is used to design another SMO to estimate the lithium-ion concentration inside the battery anode. Finally, a battery SoC estimation algorithm is developed, combining the lithium-ion concentrations (17) observed by these two observers. The parameters of the designed observer are listed in Table 3.

Table 3. Observer Parameters.

Proposed Cascade SoC Observer										
η_s	T_s	β_3	α_3	η_3	β_3	α_2	η_2	β_1	α_1	η_1
0.1	5	0.15	0.5	0.1	0.1	0.5	0.1	0.1	0.5	0.1
Proposed Cascade SoH Observer										
T_t		β_y		α_y		k_t			k_{Rf}	
5		0.9		0.5		0.15			0.0015	

An SoH estimation algorithm for Li-ion batteries is also designed. First, an augmented output dynamics is designed, as represented by (20). Then, applying Theorem 3, an observer of the augmented system is designed, as expressed in (25). Finally, an SoH estimation algorithm uses the observed power fade resistance value, as shown in (31). All relevant design parameters for this design process are also listed in Table 3.

For overall comparison, we design the SoC and SoH estimation algorithms using the conventional SMO (CSMO) method in [8] and the EKF algorithm in [7]. Battery experimental data for both DST and FUDS cycles is used for this validation. The estimation results of three different algorithms for DST and FUDS experimental data are shown in Figure 4 and Figure 5, respectively. Figures 4a,b and 5a,b presents the actual battery current, voltage signals, and estimated battery voltage outputs from three different methods. The paper's proposed observer (ITSMO) exhibits the highest accuracy in both test environments.

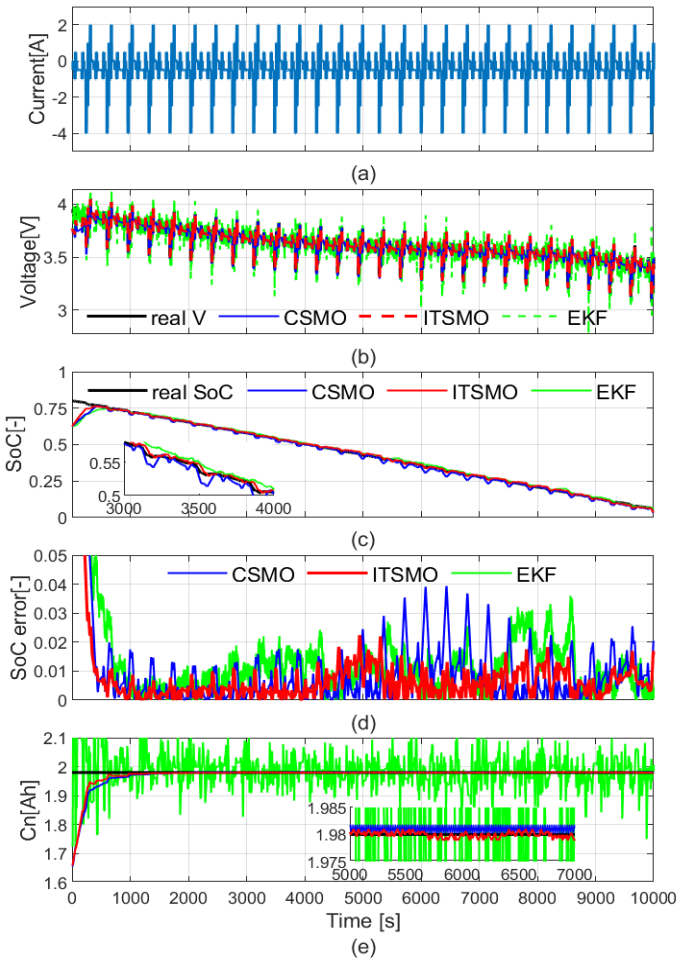

Figure 4. SoC/SoH estimation results in DST Test. (**a**) actual current; (**b**) actual and estimated voltages; (**c**) actual and estimated SoC; (**d**) SoC estimation errors; (**e**) estimates of C_n.

Figures 4c and 5c display the actual SoC under DST and FUDS tests and its estimates from the three methods. Real SoC values were determined via the Coulomb counting [8]. For all observers, the initial SoC was set at 60%.

The SoC estimation errors for each observer are shown in Figures 4d and 5d. The maximum estimation error of the proposed method (ITSMO) is less than 2.5%, and that of CSMO and EKF is less than 4% and 4.5%, respectively. Figures 4e and 5e present estimates of C_n under both test conditions. The estimates of the proposed method are most consistent with the actual values of the Li-ion battery, emphasizing its excellent accuracy.

Lastly, a quantitative evaluation of the proposed method is undertaken. Define maximum absolute error, mean absolute error, and root mean square error as follows:

$$E_{max} = \max\{|x_k|, k = 1, \ldots, n\},\ E_{mae} = \sum_{k=1}^{n} |x_k - \hat{x}_k|/n\ ,\ E_{rms} = \sqrt{\sum_{k=1}^{n} (x_k - \hat{x}_k)^2/n}$$

The performance evaluation metrics of three methods are listed in Table 4. Upon comparison, the proposed method always exhibits the smallest MaxAE, MAE, and RMSE for SoC and SoH estimates, showing its superior performance to other methods.

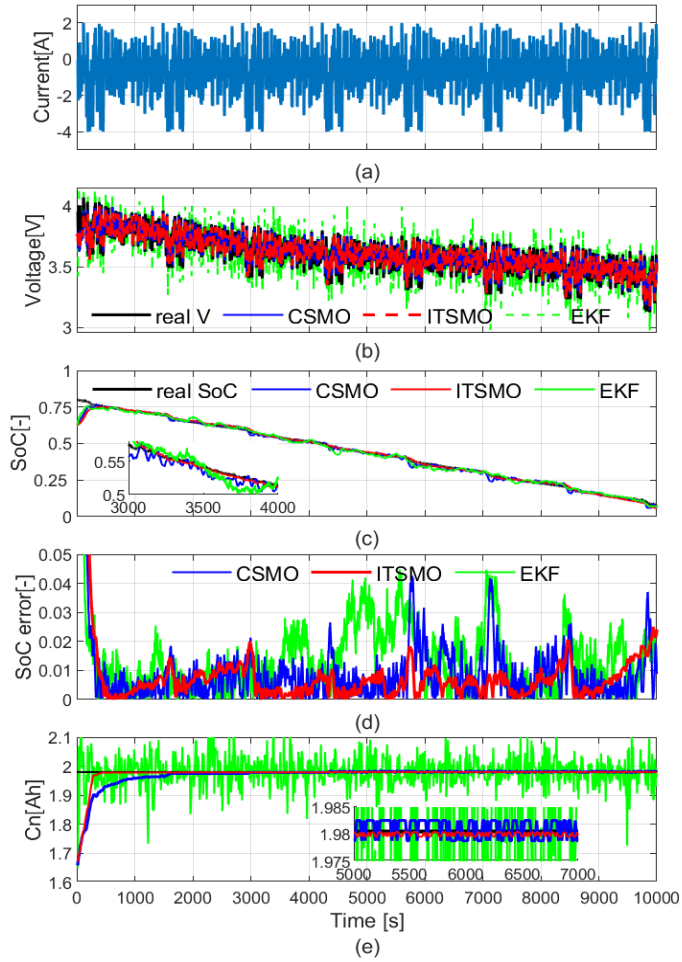

Figure 5. SoC/SoH estimation results in FUDS Test. (**a**) actual current; (**b**) actual and estimated voltages; (**c**) actual and estimated SoC; (**d**) SoC estimation errors; (**e**) estimates of C_n.

Table 4. Comparison of Estimation accuracy.

Estimate	Test	Method	E_{mae}	E_{max}	E_{rms}
SoC	DST	CSMO	0.0084	0.0394	0.0114
		ITSMO	0.0058	0.0207	0.0076
		EKF	0.0099	0.0360	0.0121
	FUDS	CSMO	0.0084	0.0426	0.0113
		ITSMO	0.0073	0.025	0.0093
		EKF	0.0133	0.0448	0.0166
SoH	DST	CSMO	0.0012	0.0047	0.0016
		ITSMO	0.0009	0.0032	0.0012
		EKF	0.0418	0.2298	0.0537
	FUDS	CSMO	0.0018	0.0025	0.0019
		ITSMO	0.0005	0.0013	0.0006
		EKF	0.0378	0.3916	0.0526

6. Conclusions

This paper proposes a new SMO-based cascade method to estimate the SoC and SoH of Li-ion batteries using SPM. This method utilizes current and voltage measurements as input to a cascade observer to accurately determine the battery anode's surface and internal lithium-ion concentrations, thereby accurately determining the SoC and SoH of the Li-ion battery. Verification through DST and FUDS experimental test data highlights the high accuracy of this method. In addition, comparative analysis with the traditional SMO method and EKF algorithm proves this method's effectiveness and superior performance, confirming its practical applicability.

Author Contributions: Conceptualization and validation, Y.F. and C.X.; methodology and resources, F.H., Z.C. and R.J.Y. All authors have read and agreed to the published version of the manuscript.

Funding: This research was supported in part by the National Natural Science Foundation of China under Grant 62073095 and in part by the Australian Research Council under Grant DP210103278.

Data Availability Statement: The original contributions presented in the study are included in the article, further inquiries can be directed to the corresponding author.

Conflicts of Interest: The authors declare no conflicts of interest.

References

1. Li, W.; Limoge, D.W.; Zhang, J.; Sauer, D.U.; Annaswamy, A.M. Estimation of potentials in lithium-ion batteries using machine learning models. *IEEE Trans. Control Syst. Technol.* **2022**, *30*, 680–695. [CrossRef]
2. Peng, Z.; Pan, C.; Yang, S.; Wen, G.; Huang, T. Finite time state-of-charge observer with robustness against unknown parameter uncertainties. *IEEE Trans. Control Syst. Technol.* **2023**, *31*, 629–636. [CrossRef]
3. Deng, Z.; Hu, X.; Lin, X.; Xu, L.; Li, J.; Guo, W. A reduced-order electrochemical model for all-solid-state batteries. *IEEE Trans. Transp. Electrif.* **2021**, *7*, 464–473. [CrossRef]
4. Gao, Y.; Liu, K.; Zhu, C.; Zhang, X.; Zhang, D. Co-estimation of state-of-charge and state-of-health for lithium-ion batteries using an enhanced electrochemical model. *IEEE Trans. Ind. Electron.* **2021**, *69*, 2684–2696. [CrossRef]
5. Moura, S.J.; Argomedo, F.B.; Klein, R.; Mirtabatabaei, A.; Krstic, M. Battery state estimation for a single particle model with electrolyte dynamics. *IEEE Trans. Control Syst. Technol.* **2016**, *25*, 453–468. [CrossRef]
6. Shehab El Din, M.; Hussein, A.A.; Abdel-Hafez, M.F. Improved battery SoC estimation accuracy using a modified UKF with an adaptive cell model under real EV operating conditions. *IEEE Trans. Transp. Electrif.* **2018**, *4*, 408–417. [CrossRef]
7. Di Domenico, D.; Stefanopoulou, A.; Fiengo, G. Lithium-ion battery state of charge and critical surface charge estimation using an electrochemical model-based extended Kalman filter. *Dyn. Syst. Meas. Control Trans. ASME* **2010**, *123*, 302–313. [CrossRef]
8. Dey, S.; Ayalew, B.; Pisu, P. Nonlinear robust observers for state-of-charge estimation of lithium-ion cells based on a reduced electrochemical model. *IEEE Trans. Control Syst. Technol.* **2015**, *23*, 1935–1942. [CrossRef]

9. Zhang, D.; Dey, S.; Couto, L.D.; Moura, S.J. Battery adaptive observer for a single-particle model with intercalation-induced stress. *IEEE Trans. Control Syst. Technol.* **2020**, *28*, 1363–1377. [CrossRef]
10. Allam, A.; Onori, S. An interconnected observer for concurrent estimation of bulk and surface concentration in the cathode and anode of a lithium-ion battery. *IEEE Trans. Ind. Electron.* **2018**, *65*, 7311–7321. [CrossRef]
11. Allam, A.; Onori, S. Online capacity estimation for lithium-ion battery cells via an electrochemical model-based adaptive interconnected observer. *IEEE Trans. Ind. Electron.* **2020**, *29*, 1636–1651. [CrossRef]
12. Doyle, M.; Fuller, T.F.; Newman, J. Modeling of galvanostatic charge and discharge of the lithium/polymer/insertion cell. *J. Electrochem. Soc.* **1993**, *140*, 1526–1533. [CrossRef]
13. Santhanagopalan, S.; White, R.E. Review of models for predicting the cycling performance of lithium ion batteries. *J. Power Sources* **2006**, *156*, 620–628. [CrossRef]
14. Tanim, T.R.; Rahn, C.D.; Wang, C.Y. State of charge estimation of a lithium-ion cell based on a temperature-dependent and electrolyte enhanced single particle model. *Energy* **2015**, *80*, 731–739. [CrossRef]
15. Feng, Y.; Xue, C.; Han, Q.-L.; Han, F.; Du, J. Robust estimation for state-of-charge and state-of-health of lithium-ion batteries using integral-type terminal sliding-mode observers. *IEEE Trans. Ind. Electron.* **2019**, *67*, 4013–4023. [CrossRef]
16. Prada, E.; Domenico, D.D.; Creff, Y.; Bernard, J.; Sauvant-Moynot, V.; Huet, F. A simplified electrochemical and thermal aging model of $LiFePO_4$-graphite li-ion batteries: Power and capacity fade simulations. *J. Electrochem. Soc.* **2013**, *160*, 616–628. [CrossRef]
17. Calce Battery Data Archive. Available online: https://calce.umd.edu/battery-data (accessed on 15 July 2023).
18. Deshpande, R.; Verbrugge, M.; Cheng, Y.T.; Wang, J.; Liu, P. Battery cycle life prediction with coupled chemical degradation and fatigue mechanics. *J. Electrochem. Soc.* **2012**, *159*, 1730–1738. [CrossRef]